Desalination and Water Treatment
www.deswater.com

doi: 10.5004/dwt.2020.25678

193 (2020) 34–47
July

Biosynthesis of silver nanoparticles and its effect on TFC RO membrane for groundwater desalination

Hosam A. Shawky[a], Rabaa Yaseen[b], Yousra H. Kotp[a,*], Doaa Eissa[c]

[a]*Egyptian Desalination Research Center of Excellence (EDRC), Desert Research Center, Cairo, P.O. Box: 11753, Egypt, Tel. +20 1063953608; Fax: +20 226389069; email: yoso20002000@yahoo.com (Y.H. Kotp)*
[b]*Department of Soil Fertility and Microbiology, Desert Research Center, El-Mataryia, Cairo, Egypt*
[c]*Department of Soil Physics and Chemistry, Desert Research Center, El-Mataryia, Cairo, Egypt*

Received 6 December 2019; Accepted 12 February 2020

ABSTRACT

In this work, silver nanoparticles (AgNPs) were produced by soil isolated fungus *Eurotium cristatum* extract and thin-film nanocomposite (Ag/PSf/PA) membrane was built-up (by adding different concentrations of AgNPs into the polysulfone support layer) to look into the impacts of nanomaterial composition (i.e., sizes, structure, and shapes) on membrane possessions and desalination operations. The desalination consequences exposed that the merging of AgNPs produced membrane of enhanced filtration performances (Ag/PSf/PA) than pure thin film composite membrane (PSf/PA). In contrast to the PSf/PA membrane, the Ag/PSf/PA membrane possesses better water flux (32 vs. 16.5 L/m^2 h) and advanced NaCl rejection (91.7% vs. 89%). Moreover, scanning electron microscopy analysis outcomes reveal that the enlargement of gram-negative (*Escherichia coli*) and gram-positive (*Listeria* sp.) were greatly inhibited on the Ag/PSf/PA nanocomposite membrane, representing the sure thing of silver nanoparticles. This analysis offers enormous potential for promising use as a new form of anti-biofouling membrane.

Keywords: Thin film nanocomposite; Silver nanoparticles; Water desalination; Anti-adhesion property; Reverse osmosis membrane

1. Introduction

Highly developed technologies might create a variation for millions of individuals around the planet challenge water contamination or water defense. The recognized superiority of membrane schemes over usual separation tools lies in the elevated separation effectiveness, low energy utilization, small paths, and eco-friendliness [1]. Reverse osmosis (RO), a pressure motivated separation progression, is hopeful nanotechnology gradually more useful for water desalination. Severe research pains have to pay attention to RO membranes and the physicochemical possessions of their shell. The recent impression "thin film nanocomposite (TFN)," which was first described in 2007 by Jeong et al. [2], refers to the relevance of nanoscale supplies inside or at the crest surface of a PA film. Since that moment, a variety of metal/metal oxides, zeolite, and carbon-based NMs have been informed in the literature, and expose improvement in TFN membranes roles. The improvement was not merely embattled at the antifouling possessions of nanocomposites, but also visible outstanding abilities to manage with the selectivity/permeability operate-off association [3]. Film fouling is able to be generally classified into three groups inorganic, organic, and biofouling [4]. In the state of biofouling, it is occurred by the addition and propagation of microorganism strains on the membrane plane, these finally form a biopolymer environment or composite structure, which is regarded a biofilm, on the membrane shell [4].

* Corresponding author.

Cairo, P.O. Box: 11753, Egypt
yoso20002000@yahoo.com

Presented at the 4th International Water Desalination Conference: Future of Water Desalination in Egypt and the Middle East, 24–27 February 2020, Cairo, Egypt

Rigorous biofouling can generate significantly dead flux, conciliated separation presentation, cleaning regularity, product pollution, quicken membrane break, and aging [5].

One of the accepted processes is by implanting the hydrophilic nanoparticles in membrane model to alter the membrane shell properties, thus, decrease fouling. The familiar nanoparticles worn to decrease fouling (particularly biofouling in opposition to bacteria) are silver (Ag) and titanium oxide (TiO_2). Few kinds of research have informed that AgNPs were used to produce low biofouling RO membranes by phase inversion system [6–9].

Silver ions and silver-supported compounds have tremendous biocidal possessions and are extensively used to organize antimicrobial plastics, burn dressings and coatings wound, etc. [10,11]. Ag self-assembled RO film prepared by phase inversion was extremely efficient alongside bacteria. But, it was established that this kind of membrane opposite a problem with a decrease of silver from membrane face [12]. The chemical reaction process was engaged to synthesize AgNPs in the existence of stabilizing mediator to keep away from the unnecessary colloids agglomeration. In toting up, AgNPs from the chemical combination is painstaking hazardous to the surroundings, costly, and use high energy [13]. In array to conquer this problem, AgNPs was prepared by the green process as it was easy and cost useful procedure [14]. A summary of fungus-mediated silver nanoparticles previously published was shown in Table 1 [15–36].

In this study silver nanoparticles was synthesized by a soil isolated fungus *Eurotium cristatum* to be used in reverse osmosis membrane production to enhance its usefulness for water desalination. The membrane structure was tested by scanning electron microscopy (SEM), transmission electron microscopy (TEM), and surface chemistry was inspected by means of energy-dispersive X-ray spectroscopy, attenuated total reflectance–Fourier transform infrared (ATR–FT-IR) spectroscopy, We also evaluate the membrane concept including water flux and salt rejection, anti-adhesion possessions of the equipped membranes was also studied by means of Gram-negative bacteria, *Escherichia coli* and Gram-positive bacteria, *Listeria* sp. as a model organism.

2. Experimental

2.1. Materials and reagents

Polysulfone (PSf, Mw = 78,000 g/mol, Density = 1.24 g/mL at 25°C) was applied from Solvay advanced polymer (Germany), N,N-dimethylacetamide (DMAC, 99.8%, Density = 0.94 g/mL at 20°C) as solvent was supplied from Fisher (USA), m-phenylenediamine (MPD, 499%), trimesoyl chloride (TMC, 498.5%), and hexane (high performance liquid chromatography grade, 97%) were all got from Sigma-Aldrich (USA) (silver nitrate ($AgNO_3$) sodium chloride (NaCl) was obtained from Uni-Chem, and nitric acid (HNO_3, 69%) was

Table 1
Overview of fungus-mediated silver nanoparticles

Fungi	Size (nm)	Shape	Application	References
Fusarium acuminatum	5–15	Spherical	–	[15]
Aspergillus flavus	8.92	Not available	–	[16]
Fusarium oxysporum	15–20	Spherical	Antibacterial	[17]
Fusarium oxysporum	21.3–37.3	Spherical and oval	Antimicrobial	[18]
Trichoderma asperellum	13–18	Not available	–	[19]
Penicillium sp.	52–104	Not available	–	[20]
Penicillium decumbens	30	Spherical	Anticancer	[21]
Fusarium culmorum	5–25	Spherical	–	[22]
Aspergillus clavatus	10–25	Spherical or hexagonal	–	[23]
Amylomyces rouxii	5–27	Spherical	Antimicrobial	[24]
Neurospora crassa	11	Spherical	–	[25]
Trichoderma reesei	5–50	Not available	–	[26]
Inonotus obliquus	14.7–35.2	Spherical	Antibacterial, antioxidant and antiproliferative	[27]
Trichoderma harzianum	10–51	Cubic	Antibacterial	[28]
Aspergillus oryzae	6–26	Spherical	–	[29]
Metarhizium anisopliae	28–38	Rod-like	Insecticidal	[30]
Aspergillus terreus	8–20	Spherical	Antimicrobial	[31]
Monascus purpureus	1–7	Not available	Anti-Candida	[32]
Colletotrichum sp.	20–50	Myriad shapes (spherical, triangular and hexagonal)	Antibacterial	[33]
Aspergillus fumigatus	23	Spherical	Antibacterial	[34]
Duddingtonia flagrans	14.51	Spherical	Nematicidal	[35]
Terminalia fagifolia		Spherical or polygonal	–	[36]
Eurotium cristatum	16.56	Spherical	Desalination	This study

provided by VWR Chemicals (Dorset, UK). Media from Oxoid (UK). Water (18.2 MΩ cm at 25°C) used to prepare all solutions were purified with a NANO pure® Diamond™ UV water system. All the materials needed for microbiological experiments were purchased from HIMEDIA (India), including the component of Yeast Extract–Malt Extract Broth medium, glucose 10 g/L, sucrose 10 g/L, malt extract 3 g/L, yeast extract 3 g/L, peptone 5 g/L, pH value = 7.2. All reagents and chemicals utilized in this research were of systematic grade purity.

2.2. Isolation, identification, and fungal biomass production

The soil isolate, *E. cristatum* previously secluded from the soil and was known to utilize its cultural characteristics. The clean culture of fungus was worn for biomass fabrication. *E. cristatum* fungus was vaccinating in 250 mL Erlenmeyer flask containing Yeast Extract–Malt Extract broth medium broth medium. The vaccinated medium was kept warm at 30°C on revolving shaker at 120 rpm. After incubation of 72 h, the fungal mat was estranged by filtration, cleaned thrice with sterile distilled water and dried at 50°C. The collected fungal mat was used for silver nanoparticle synthesis.

2.3. Biosynthesis and characterization of silver nanoparticles by isolated fungi

One g of fungal biomass was inoculated into 250 mL Erlenmeyer flask containing 50 mL of 100 mM silver nitrate solution and incubated at 45°C for 48 h at dark. Control made without fungal biomass. After incubation, the solution was cleaned and the particle size of silver was calculated. TEM (JEOL GEM-1010 TEM at 70 kV at the Regional Center for Mycology and Biotechnology (RCMB), Al-Azhar University) was used to determine the morphology and size allocation of the freshly manufactured AgNPs. The absorption peak of silver nanoparticles was observed using UV-visible (UV-Vis) spectrophotometer (Elico EI 301E, India). The functional groups on the level surface of silver particles were estimated by Fourier transform infrared (FT-IR) spectroscopy (Nicolet avatar 230 spectrometers) at room temperature. Powder X-ray diffraction (XRD) patterns were made by (Shimadzu X-ray diffractometer, Model XD 490 Shimadzu, Japan).

2.4. Preparation of PSf synthesis of PSf and Ag/PSf support layers

The PSf support layer (16 wt.% in DMA) was prepared derived from our previous study [37]. The amount of silver nanoparticles (AgNPs) varied from 0.0 to 0.3 wt.% was added to a PSf solution, followed by sonication for 1 h, A thin PSf film was cast by spreading the PSf solution on top of a glass platter by a casting blade. The produced film was deep in deionized water at 298 K. The resultant PSf support membrane be rinsed and reserved in deionized water (DI) water and washed before further use.

2.5. Preparation of PSf/PA and Ag/PSf/PA membranes

Control PSf/PA and Ag/PSf/PA membranes were fabricated using the PSf substrate directly. The PSf membrane contained no AgNPs and Ag/PSf containing different concentrations of AgNPs were engrossed in an aqueous solution of 2.0 wt.% MPD for 2 min. Excess solution on the surface was removed by a rubber roller. Next, the MPD saturated PSf and Ag/PSf support layer was soaked in an organic solution of 0.15 wt.% of TMC-hexane for 60 s, completing the construction of a polyamide (PA) film. The equipped membranes were cleaned with DI water before testing.

2.6. Membrane characterization and performance evaluation

SEM examination of membrane shell was conducted through an SEM Model Quanta field emission gun with an accelerating voltage of 30 kV. EDX microanalysis was conceded by X-ray micro-analyzer (Oxford 6587 INCA) emotionally involved to JEOL JSM-5500 LV (Japan) SEM at 20 kV at the RCMB, Al-Azhar University. To obtain the TEM, electron micrographs were obtained using JEOL GEM-1010 TEM at 70 kV at the RCMB, Al-Azhar Univerity. The hydrophilicity of films surface was assessed utilizing a VCA Video Contact Angle System (Kr ÜssDSA25B, Germany). The functional groups on the surface of the membranes were assessed by FT-IR spectroscopy (Nicolet avatar 230 spectrometers, Japan) at room temperature. XRD models of different membranes were examined by (Shimadzu X-ray diffractometer, Model XD 490 Shimadzu, Japan).

To illustrate the mechanical properties of the modified membranes, their elongation and tensile strength properties were firmed by dynamic mechanical analysis (DMA) utilizing a universal mechanical testing instrument (DMATAQ800) (film tension clamp). Estimations were performed at 25°C with a strain rate of 50 mm/min.

2.7. Separation performance testing

A high-pressure cross-flow filtration system, similar to the one reported by Kotp et al. [38] was used to evaluate water flux and solute rejection of membranes under different pressure. For each test, a membrane coupon with an effective area of 2.4 cm^2 was located in a filter holder. The indication was pre-compressed with DI water at the put pressure of 10 bar for 2 h to attain a steady water flux. All membrane models were prepared and tested at slightest twice with three membrane tests for RO performance. The water flux (F) was computed using Eq. (1):

$$F = \frac{V}{At} \tag{1}$$

where V is the total volume of permeated pure water (L), A is the valuable membrane area (m^2), and t is the operation time (h). The rejection (R) was calculated with NaCl (2,000 ppm) and computed using Eq. (2):

$$R = \left(1 - \frac{C_p}{C_f}\right) \times 100 \tag{2}$$

where C_p, C_f is the concentration of the permeate and feed water, respectively.

Reusability of the PSf/PA and Ag/PSf/PA films after cleaning with water rising was considered by successive

cycles. For this reason, 250 mL of citric acid (2 wt.%) was used as desorption arrangements. To start with, films were equilibrated with NaCl arrangement then they were put into the desorption arrangements and shaken for 24 h. After the desorption stage, the layer was used over again in an adsorption strategy, as depicted previously.

2.8. Water sampling and laboratory analyses

One field trip in Matrouh district was led in June 2018 for water inspection and distinctive field estimations. One water test was gathered from the examined zone. Distinctive concoction investigation of gathered water tests was finished at the central lab of the Desert Exploration Center in Cairo, Egypt. The pH and electrical conductivity (EC) were painstaking in the field tour through convenient pH and EC meters (Hanna Instruments, Ann Arbor, Michigan, USA). The water tests were positioned in 1,000 mL limit polyethylene bottles. The water tests were pruned and dissected in the research facility for significant particles (Ca^{2+}, Mg^{2+}, Na^{+}, K^{+}, $HCO_3^{\bullet-}$, CO_3^{-}, $SO_4^{\bullet 2-}$, Cl^{-}) utilizing standard techniques [37]. Salt metal particles sodium (Na^{+}) and potassium (K^{+}) were set utilizing a fire photometer (Jenway PFP 7, UK). All out hardness (TH), and calcium (Ca^{2+}) were set titrimetrically utilizing the run of the mill EDTA measures. Carbonate (CO_3) and bicarbonate ($HCO_3^{\bullet-}$) were determined by volumetric strategies. Magnesium (Mg^{2+}) was determined from TH and Ca^{2+} substance. Chloride was tested by $AgNO_3$ titration. The turbid measurement procedure was used for the assessment of sulfate [37].

2.9. Bacterial tests

Anti-adhesion test was directed with gram-negative (*E. coli*) and gram-positive (*Listeria* sp.) which are segregated from Matrouh territory. The readied microscopic organisms were then weakened up to multiple times with PBS to get a suspension of about 30×10^2 cells/mL for *E. coli* and 80×10^2 for *Listeria* sp. In the underlying attachment tests, PSf/PA, and Ag/PSf/PA films (d = 20 mm) were drenched together into both the *E. coli* and *Listeria* sp. suspension (10 mL) in a fixed container and the blend was shaken in a hatchery shaker at 200 rpm and 37°C for 6 h. From that point onward, the films were washed multiple times delicately with PBS. The microorganisms stayed on each sort of the films were seen with SEM as a sign of bacterial bond. Before the SEM examine, the examples were set up as pursues [39] every film test was soaked into 3% (v/v) glutaraldehyde arrangement at 4°C for the obsession of the followed microscopic organisms. After 3 h, the film was removed from the glutaraldehyde arrangement, trailed by step lack of hydration with 100% ethanol. The layer was then dehydrated at 25°C to be prepared for SEM examine.

3. Results and discussion

3.1. Characterization of AgNPs

TEM examination of the silver nanoparticles used in this work Fig. 1a. illustrated that the particles be likely to be well isolated and of spherical morphology. The common diameter was 16.56 nm. Thus, the existence of silver nanoparticles was depicted using UV-Vis spectrometer as illustrated in Fig. 1b. The Only broad peak was observed, centered at 418 and 436 nm which matched to the plasmon excitation of the silver nanoparticles [40]. It is normally established that the absorption peak whose maximum occurs at around 418 nm is related to the configuration of silver metal particles as well as the distance between the neighboring nanoparticles, and its height corresponds to the concentration of the silver metal particles and indicate Ag particles with a uniform nanosize be present in the Ag colloid solution [41,42].

Fig. 1c illustrates the FT-IR spectrum obtained from the freeze-dried concentrate of silver nanoparticles, produced after 72 h of incubation with the fungus. The amide connection among amino acid remains in proteins provide rise to the recognized marks in the infrared area of the electromagnetic band. The bands were seen at 3,420 and 2,921 cm^{-1} were assigned to the stretching vibrations of primary and secondary amines, correspondingly, while their corresponding bending vibrations were spotted at 1,698 and 1,558 cm^{-1}, respectively. The two bands observed at 1,380 and 1,026 cm^{-1} be able to be appointed to the C–N stretching vibrations of aromatic and aliphatic amines, respectively. The general study confirms the occurrence of protein in the sections of silver nanoparticles. It is reported earlier that proteins can bind to nanoparticles either through free amine groups or cysteine residues in the proteins [16,43,44] and via the electrostatic attraction of negatively charged carboxylate groups in enzymes occurred in the cell partition of mycelia as a result, stabilization of the silver nanoparticles by protein is a possibility. XRD pattern of the obtained silver nanoparticles. Fig. 1d. In XRD spectrum the diffractions at 32°, 41.2°, and 67.2° 2θ can be referred to the (111), (200), and (220) planes of the features-centered silver, respectively. While two new peaks (*) are formed owing to the communication of silver with the fungal cell partition.

3.2. Membrane characteristic

Surface and cross-section of PSf/PA and Ag/PSf/PA membranes were observed by SEM images Fig. 2. It showed that Ag/PSf/PA membrane had the same ridge-and-valley structure of a PSf/PA membrane. At a relatively high magnification of 20,000, deposits of bright nanoparticles can be observed on the membrane surfaces. The SEM analysis coupled with EDX definitude the formation of discrete silver nanoparticles instead of a continuous layer of Ag^0 deposits on the PSf support membrane (Fig. 2b). The nanoparticles, however, were unevenly spread at the microscale and varied in diameter. Most AgNPs contain size fewer than 20 nm, but they are capable of form aggregates with diameters up to 180 nm in the interior membrane. TEM images and EDX spectra are presented for PSf/PA and Ag/PSf/PA membranes in Figs. 3a and b. Both PSf/PA and Ag/PSf/PA membranes exhibit nano-scale surface roughness, which is a well-known characteristic of interfacially polymerized polyamide RO membranes [24,28]. The asymmetrical morphology permits quantification of a single film layer thickness, but equally thin films are about 40–200 nm. In Fig. 3b, silver nanoparticles appear considerably darker than the polymer and are located within the cross-section of the

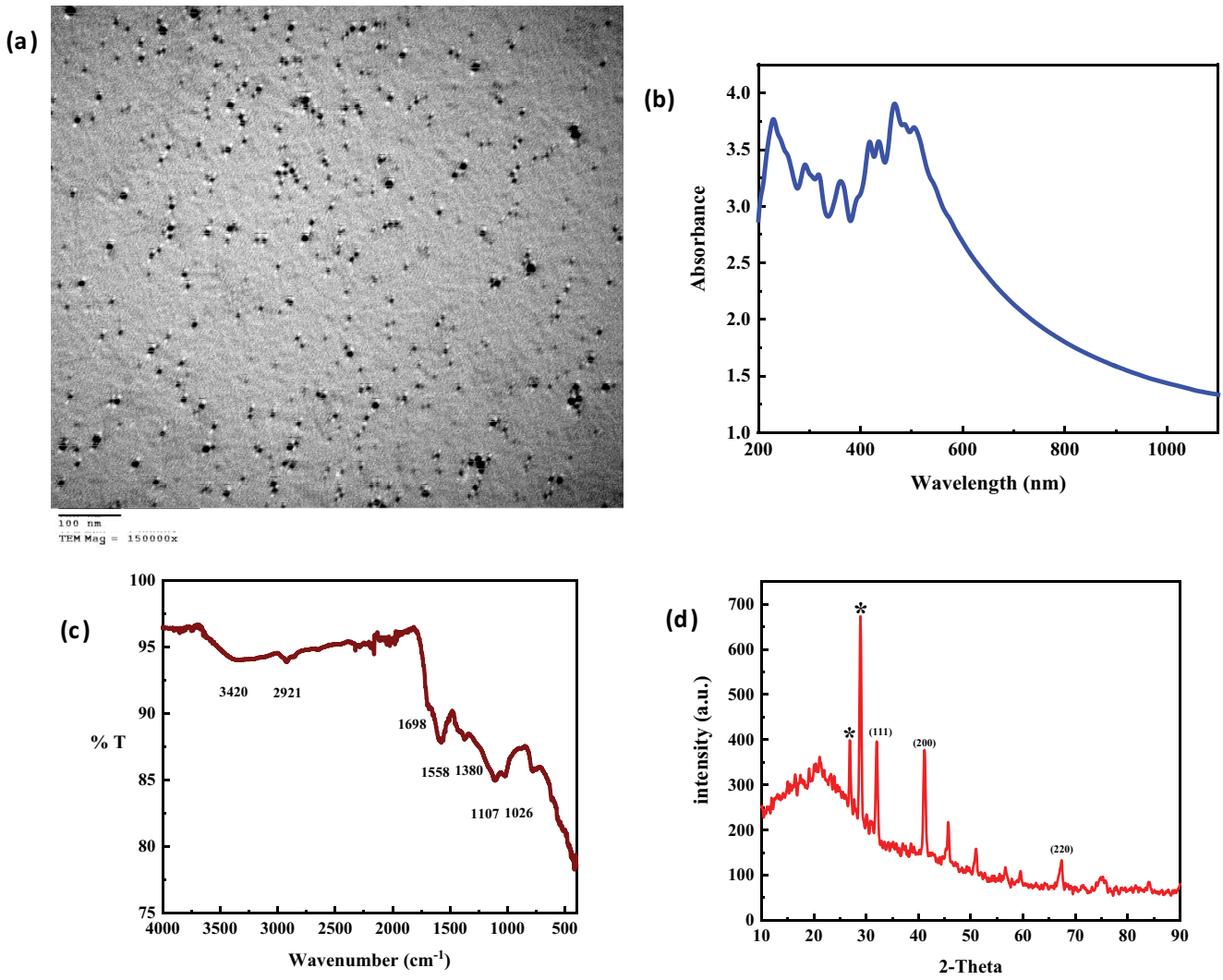

Fig. 1. TEM image of AgNPs (a), UV-vis absorption spectrum (b), FT-IR spectra (c), and XRD pattern of AgNPs (d).

thin film Fig. 2d, and also at the border. The EDX scale in Fig. 3b indicates the appearance of the characteristic silver peak in the EDX structure also established the existence of Ag nanoparticle in the PSf support besides the presence of sulfur peak from the PSf support.

Surface crystallization of PSf/PA and Ag/PSf/PA membrane were evaluated by XRD, as shown in Fig. 4. XRD models of PSf/PA (containing Zero Ag nanoparticles in the PSf support layer) and Ag/PSf/PA (containing Ag nanoparticles in the PSf support layer) membranes. (Fig. 4) differed with deference to Ag nanoparticles related peaks. The XRD pattern of the Ag/PSf/PA membrane exhibited three diffraction peaks for silver: Ag (1 1 1) and Ag (2 0 0) [45], these peaks were absent in the XRD patterns of the PSf/PA membrane.

FT-IR spectra of PSf support layer, PSf/PA, and Ag/PSf/PA membranes are shown in Fig. 5. For the PSf support layer, peaks at 1,586 and 1,486 cm^{-1} could be assigned to aromatic C–C stretching, 1,324 and 1,219 cm^{-1} to the doublet from the asymmetric O=S=O stretching of sulfone group, 1,231 cm^{-1} to the asymmetric C–O–C stretching of aryl ether group and 1,172 cm^{-1} to the symmetric O=S=O stretching of sulfone group, all existing in the PSf fractious-linking polymerization [38]. For PSf/PA thin layer was coated on the PSF support layer following the IP process, and several new peaks appeared on the spectrum (Fig. 5). Peaks at 1,638 cm^{-1} (amide I, C=O stretching vibrations of amide), 1,577 cm^{-1} (amide II, in-plane N–H bending and C–N stretching vibrations), 1,614 cm^{-1} (N–H stretching of amide II) and 1,444 cm^{-1} for (C=O stretching and hydroxyl bending of carboxylic acid) were created from the polymerization of PA and included amide implementations [46–48]. Besides these peaks from PA thin-film layer, the peak between 2,852 and 2,923 cm^{-1} derived from the asymmetric and symmetric vibration of CH_2 groups in *E. cristatum* fungus [49–51], while their bending vibrations of primary and secondary amines were distinguished at 1,712 and 1,541 cm^{-1}, respectively, these both bands are narrow and intense in AgNPs spectrum relative to the spectrum of fungous extract. The stretching band at 3,337 cm^{-1} assures the presence of either OH groups of algal polysaccharides or –NH groups of amide. However, this band is more intense and is transferred to a higher wavenumber (3,420 cm^{-1}) in the

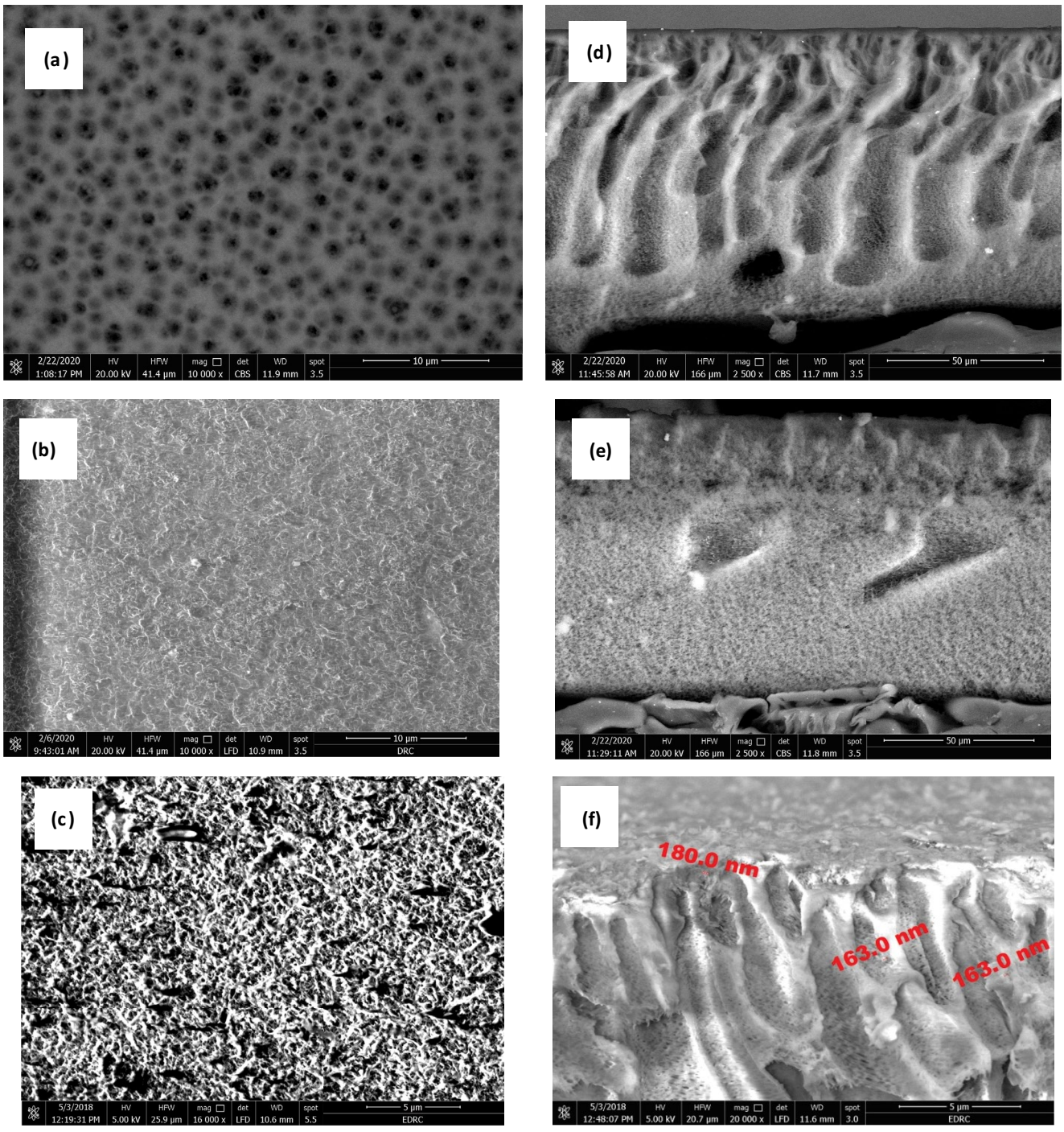

Fig. 2. SEM images of top surface (a–c) and cross section (d–f) of PSf, PSf/PA, and Ag/PSf/PA nanocomposite RO membrane, respectively.

spectrum of AgNPs [52–54]. The metal-polymer communication bands are spotted specifically in the little frequency state (600–400 cm^{-1}). Silver exhibits a distinct new band at 626 cm^{-1} (owing to metal-oxygen interaction) and a small shoulder band at 871 cm^{-1}. Thus, from the FT-IR spectra, one can observe that metals have exposed relations with the electron contributed sites, that is, oxygen sites present in the polymer spine [55].

To study the hydrophilicity of the prepared membranes, the contact angle mensuration was performed. The contact angle value signifies the affinity of water to dabble the membrane surface. The lesser contact angle points to the superior affinity for water to dabble the membrane and the better hydrophilicity. As presented in Fig. 6, the contact angle of Ag/PSf/PA membrane is smaller than PSf/PA membrane, the contact angle value reached 40° that corresponds

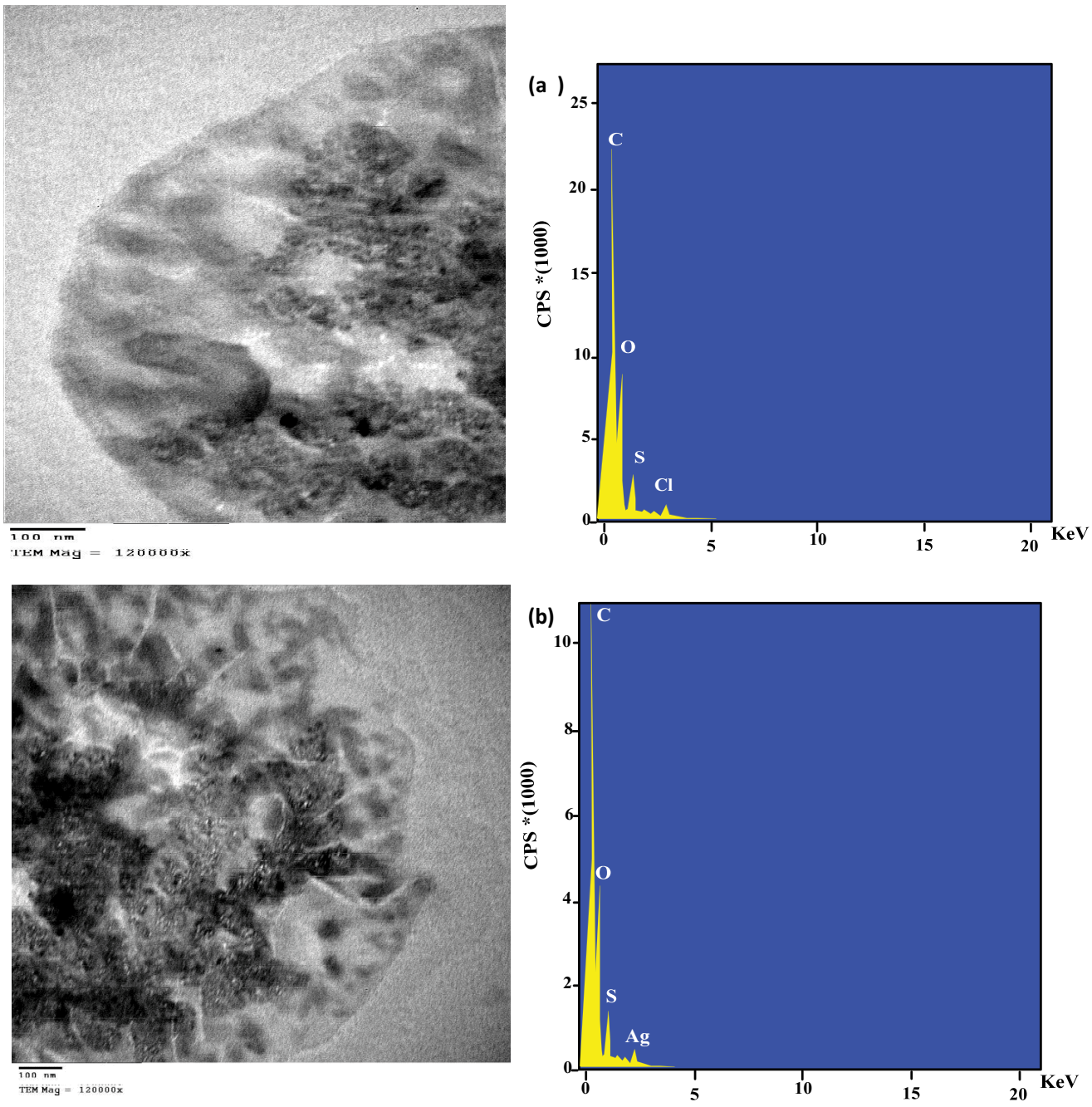

Fig. 3. TEM and EDX images of PSf/PA (a) and Ag/PSf/PA (b) nanocomposite RO membrane, respectively.

to the reduction by 35% compared to PSf/PA membrane. The decrease of the contact angle of the Ag/PSf/PA membrane can be explained by the increase of the surface charge density [56].

The mechanical features are crucial for the RO substrates because the RO process works under elevated pressures. This places of interest the essential to synthesize mechanically tough membranes. The stress-strain plots of PSf, PSf/PA, and Ag/PSf/PA membrane membranes are presented in Fig. 7, while the mechanical strength data are summarized in Table 2. The tensile strength of PSf, PSf/PA, and Ag/PSf/PA membrane membranes were 8.03, 10.92, and 9.74 MPa, with a corresponding Young's modulus of 299.9, 621.8, and 643.4 MPa, respectively. The doping of a small quantity of Ag into PSf membrane and coating it with a thin film of polyamide layer increased the tensile strength of the PSf support membranes to 9.74 MPa, ensuing in Young's modulus of 643.4 MPa. The Young's modulus of the membrane samples was determined at their elastic region. This result demonstrated that the coating of Ag/PSf membrane with PA layer improved their mechanical force as was before announced [57]. The tensile strength and elongation of Ag/

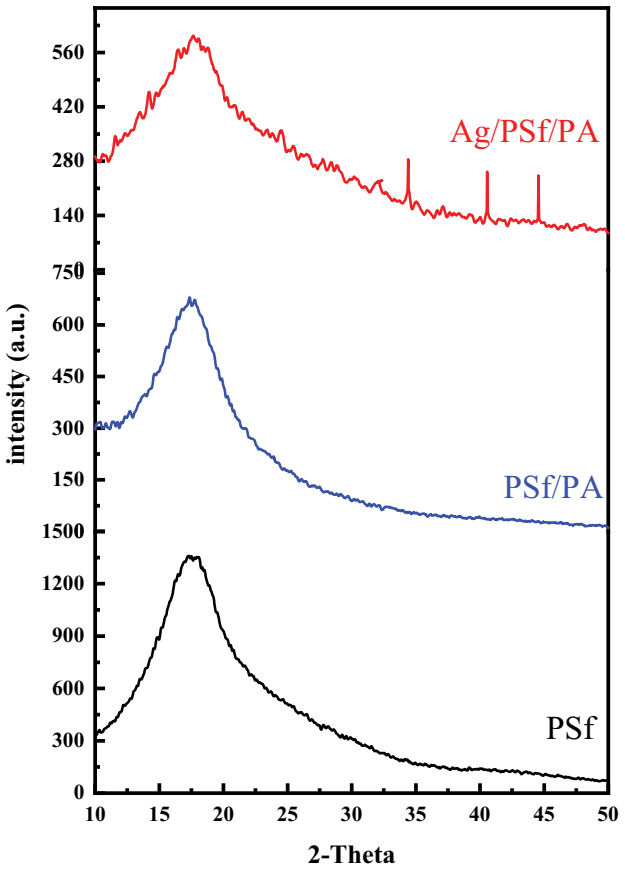

Fig.4. XRD images of PSf, PSf/PA, and Ag/PSf/PA nanocomposite RO membrane.

PSf/PA decreased than the membrane prepared with PSf/PA, this may be explained by the addition of nanoparticles increased the porosity of membrane as mentioned before [58].

3.3. Performance of PSf/PA and Ag/PSf/PA membrane

Permeate flux from 2,000 mg/L NaCl solution and salt rejections of the PSf/PA and Ag/PSf/PA membranes were measured at 10 bar (Fig. 8). Ag/PSf/PA membrane rejected NaCl at 91.7%, which was greatly higher than the salt rejections of the PSf/PA (89%). It appears that the nano-porous

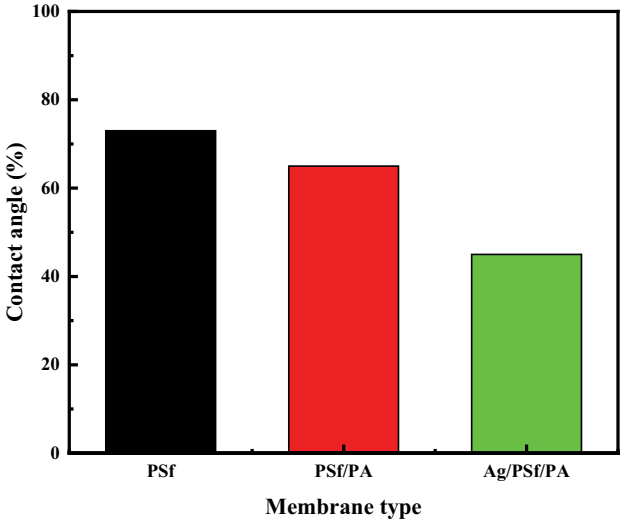

Fig. 6. Contact angles results of the surface of PSf, PSf/PA, and Ag/PSf/PA membranes.

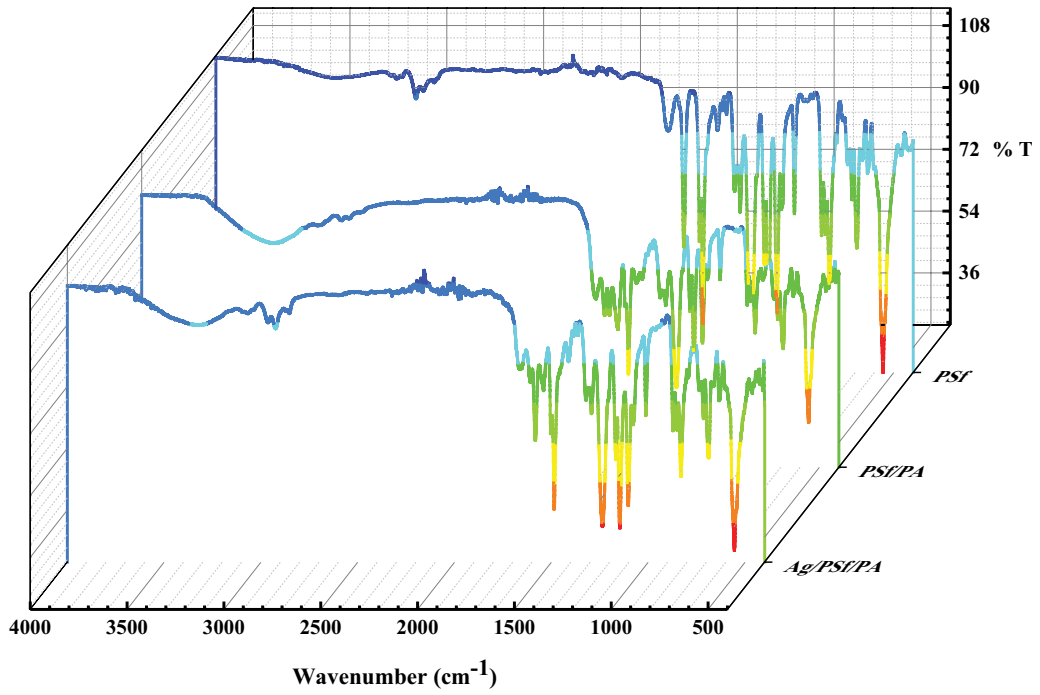

Fig. 5. FT-IR spectra of PSf, PSf/PA, and Ag/PSf/PA membranes.

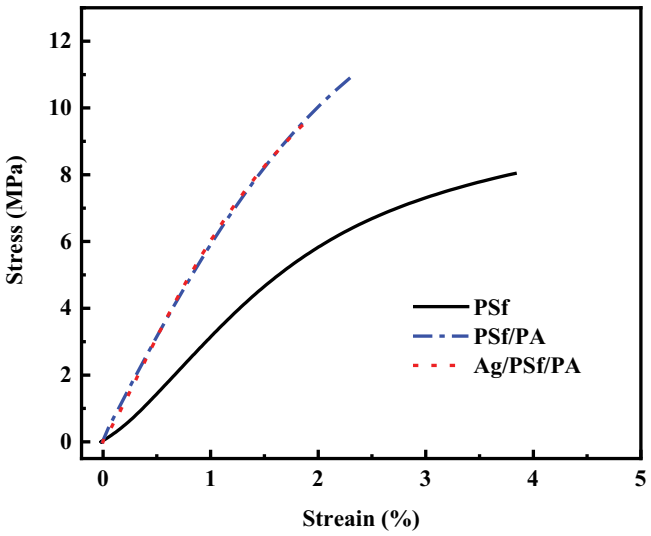

Fig. 7. DMA curves show stress and strain of PSf, PSf/PA, and Ag/PSf/PA membranes.

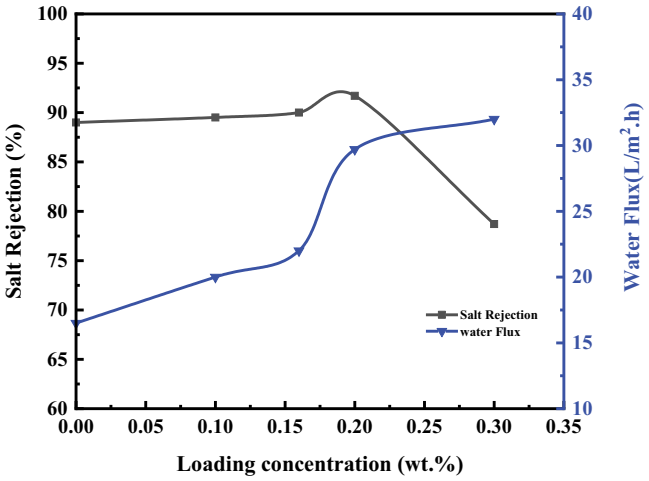

Fig. 8. Effect of AgNPs concentration on salt rejection and water flux of the resulting Ag/PSf/PA membrane testing with 2,000 mg/L NaCl aqueous solution at 10 bar, 25°C (after 60 min).

constitution of PSf support layer did not permit major salt rejection. Following the IP process, these nano-pores were covered by a PA thin-film layer, which acted as a dense barrier or ejects salt ions. For the Ag/PSf/PA membranes, the permeate flux increased from 16.5 to 32 L/m² h (a 100% increase) with increasing AgNPs concentration from 0 to 0.3 wt.%. It can be caused by the increase of membrane hydrophilicity because the elevated hydrophilicity helps the solubilization and distribution of water jot inside the membrane. Moreover, the AgNPs entrenched in PSf support layer be able to alter the cross-linking state of the polymer medium during producing microporous imperfection. Moreover, the internal pores of Ag/PSf/PA could enhance the water permeability by providing short flow paths for water molecules. Clearly, the membrane equipped by using 0.2 wt.% of AgNPs was considered optimal, since the water flux increased with further concentration increases. The decreasing in salt rejection with increasing silver nanoparticle loading might be happened by the accumulation of AgNPs, which might take place more simply at a larger concentration. The aggregation could concern the spreading of NPs in the PSf support layer, where due to the aggregation of filler, fewer water uptakes and holey fluxes were spotted with higher capacity of filler in the PSf support layer.

Furthermore, the effect of the operating pressure and NaCl concentration on Ag/PSf/PA RO rejection and flux are also considered. Fig. 9 shows that the flux of the Ag/PSf/PA membrane increase with an increase of operating pressure.

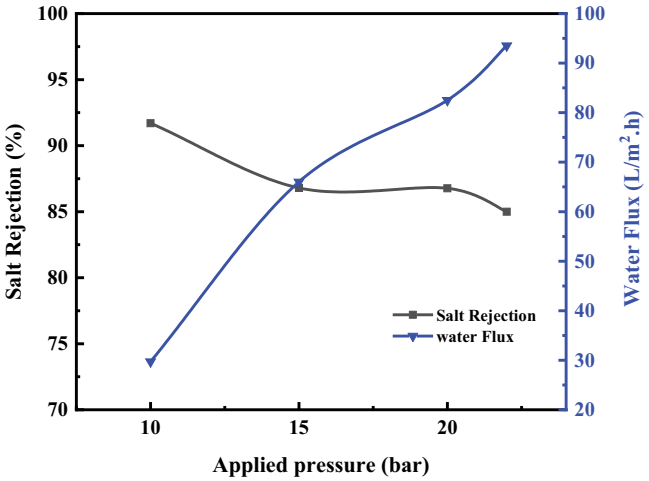

Fig. 9. Pure water flux as a function of operating pressure for the Ag/PSf/PA nanocomposite membrane.

This agrees with the Kimura–Sourirajan analysis of RO membrane transport [59]. But the salt rejection decrease and the link between the flux and the working pressure is nearly linear.

The salt rejection rate and water flux of Ag/PSf/PA membrane are tested under different feed NaCl concentrations at 12 bar and 25°C and the results are shown in Fig. 10. It is clear that with the feed concentration rising, the

Table 2
Mechanical properties of PSF, PSF/PA, and Ag/PSF/PA membranes

Membrane samples	Thickness (μm)	Tensile strength (MPa)	Young's modulus (MPa)	Elongation (%)
PSf	170	8.03	299.90	3.81
PSf/PA	160	10.92	621.80	2.30
Ag/PSF/PA	160	9.74	643.40	1.92

rejection rate of the membranes primary betake at lesser salt concentration and then betake down when the salt concentration goes above about 2,000 mg/L, as the water flux of the composite membranes goes down since the rise of the osmotic pressure. Moreover, therefore, the Ag/PSf/PA membrane is generally suitable to process the aqueous solutions with low salt concentration such as brackish water.

3.4. Application of the resulting Ag/PSf/PA membrane on real groundwater

A groundwater sample from Marsa Matrouh, on the northwestern coast of Egypt, has been functioning as a water basis to the RO direct system utilizing the prepared flat sheets Ag/PSf/PA membrane. The different kind of product water through the Lab. RO unit was investigated for the major ion ingredients to define the performance of every membrane through 15 bar applied pressure, at a constant temperature of (25°C), and also fixed flow rate about (5 L/min), a brief result of feed and product water examination outcomes are observed in Table 3. From results, the salt rejections of (Mg^{2+} and SO_4^{2-}) divalent ions are superior to the rejection of (Na^+ and Cl^-) monovalent ions, where the retention for the divalent anions is less than cations ions. This can be established by the coefficients of mass transfer for divalent ions are lesser than those for the monovalent ions and hence superior values for solute separations with admiration to divalent ions [60]. Moreover, the quantity of hydration which is a meaning of equal size and charge/existence greater for small ions with a great charge, since there is a sturdy interaction of the solute ions with water molecules (ion dipole influence) [61].

The Ag/PSf/PA membrane exhibited noteworthy groundwater fluxes of above 29.7 L/m² h, while that flux for TFC membrane was about 16.5 L/m² h (Fig. 8). In spite of its outstanding capability to eliminate dissolved ions, the effectiveness of the RO membrane for the exclusion of undissociated little molecular weight (MW) solutes, such as strontium (17.95 ppm), Table 2 has yet to achieve a satisfactory level. The existence of Sr is undesired as it can threaten not only public health, other than the environment.

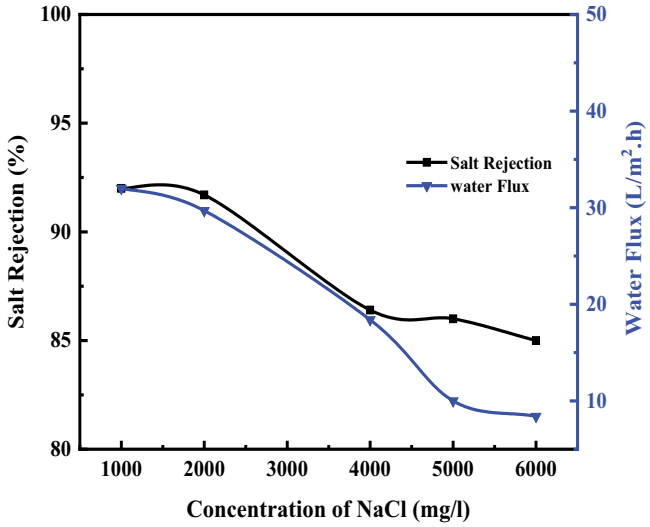

Fig. 10. Effect of salt concentration on the salt rejection rate and water flux of the resulting Ag/PSf/PA membrane.

Table 3
Brackish groundwater characters before and after desalination process at 20 bar operation pressure

Analytical parameter (mg/L)	Feed water samples results	Product water results	
	Brackish water	PSf/PA	Ag/PS/PA
TDS	8,090	973	656
Na^+	1,050	120	110
K^+	200	8	8
Mg^{2+}	150.0	15.3	13.0
Ca^{2+}	100.0	16.8	16.8
CO_3^{-2}	12.0	0	0
HCO_3^-	120.0	90.0	85.4
SO_4^{2-}	364.0	86.0	30.0
Cl^-	2,149.0	219.0	170.0
B	1.3	0	0
Cu	0.02	0	0
Fe	0.12	0	0
Li	0.11	0	0
Mn	0.16	0	0
Ni	0.08	0	0
Si	11.97	1.2	0.96
Sr	17.95	1.94	1.3
V	0.01	0	0

3.5. Reusability of PSf/PA and Ag/PSf/PA membranes

PSf/PA membrane is very sensitive to disinfecting agents, especially oxidizers such as chlorine. More studies have been completed relating to the effects of pretreatment and cleaning chemicals on polyamide membrane degradation. Specifically, monochloramines, sodium hypochlorite, potassium permanganate hydrogen peroxide, and sodium hydroxide in association with sodium laurel sulfate and the catalytic possessions of Fe and Al in RO membranes oxidation. Moderately small awareness has been rewarded to the part of membrane regeneration and reuse, and few papers address this topic [62–66]. Experiments to measure the reusability of membranes were executed, and herein 2 wt.% citric acid is used as an organic solvent for 24 h. This was fairly effective in maintaining acceptable flux performance for a long time [67]. At least five numbers of cycles are wanted to create the process more economic.

Here, the morals of water flux and salt rejection properties are computed by the parameters of the different circles of membrane and washing. As seen in Fig. 11 the water flux value of Ag/PSf/PA hybrid membrane is the highest, and that of PSf/PA membrane is the lowest. PSf/PA and Ag/PSf/PA membranes after three cycles maintain their capability for its permeability with a slight loss in the salt rejection. Salt rejection quantities are decreased quickly for the third sequence. Hence, the amount of duplicate cycles might be sufficient to motivate the reusability of the membranes. However, whole desorption (100%) was not attainable possibly since of the stable trap of NaCl moieties in the polymer backbone [68]. Furthermore, the elevated the hydrophilicity, the better the anti-scaling performance. As a result, it can illuminate that the accumulation of elevated hydrophilic Ag nanoparticles has the maximum development on the capability of inorganic fouling opposition of membranes this was moderately effective in maintaining acceptable flux performance for a long time.

3.6. Anti-adhesion properties

Anti-adhesion effects. The number of adhered bacteria on the customized membranes decreased significantly with admiration to the unspoiled membrane, highlighting the brilliant anti-adhesion capacity of the modified membranes. The connection of model biofilm for microorganisms, *E. coli* and *Listeria* sp., was studied in arrange to demonstrate bacterial repellence performance of both *E. coli* and *Listeria* sp., membranes. The lower CFU values indicate stronger bactericidal effects or bacterial repellence (anti-adhesion). Fig. 12 illustrates the attachment of *E. coli* and *Listeria* sp., on PSf/PA and Ag/PSf/PA membranes, In general, the CFU test detected a lower number of the adhered *E. coli* and *Listeria* sp. on Ag/PSf/PA membrane surfaces. In reality, the CFU results exposed that the connection of *E. coli* and *Listeria* sp. were significantly dissimilar among the specimens. The consequence of the surface possessions can be noticed on the connection of bacteria, since an obvious connection between the enhancement in hydrophilicity (Fig. 6) and likewise, a decline in the connection of the bacteria. Furthermore, the lesser surface roughness may have exaggerated on the bacterial attachment. Therefore, Ag/PSf/PA revealed anti-adhesion and bacteria repellence performance, due to the physiochemical anti-fouling performance. However, Ag/PSf/PA showed also hydrophilic and smooth surface roughness. This suggested that the powerful effect on the connection of bacteria was attained by joining the antimicrobial action with the physiochemical anti-adhesion surface properties [69].

4. Conclusion

Our work presents a simple and facile biosynthesis approach of AgNPs from soil isolated fungus *E. cristatum* extract. TFN (Ag/PSf/PA) membrane was developed (by incorporating AgNPs into the PSf support layer. The research focuses onto recognize the interactions linking the AgNPs and the PSf support layer and survey the AgNPs effectiveness on the physicochemical properties and the desalination performance of the fabricated membranes. PSf/PA and Ag/PSf/PA membranes evidenced by detailed characterizations (TEM, SEM, XRD, DMA, and FT-IR). The water flux was significantly increased by approximately 100% using the 0.2 wt.% AgNPs incorporated Ag/PSf/PA membrane while the salt rejection increased slightly. The merging of AgNPs

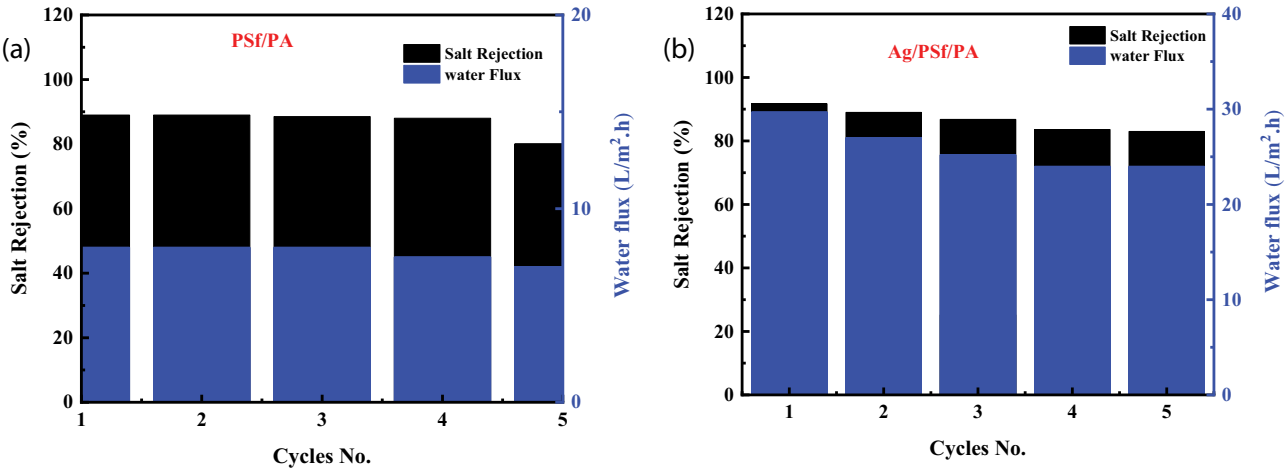

Fig. 11. Salt rejection and water flux of PSf/PA and Ag/PSf/PA membranes treated with 2 wt.% citric acid at different cycles.

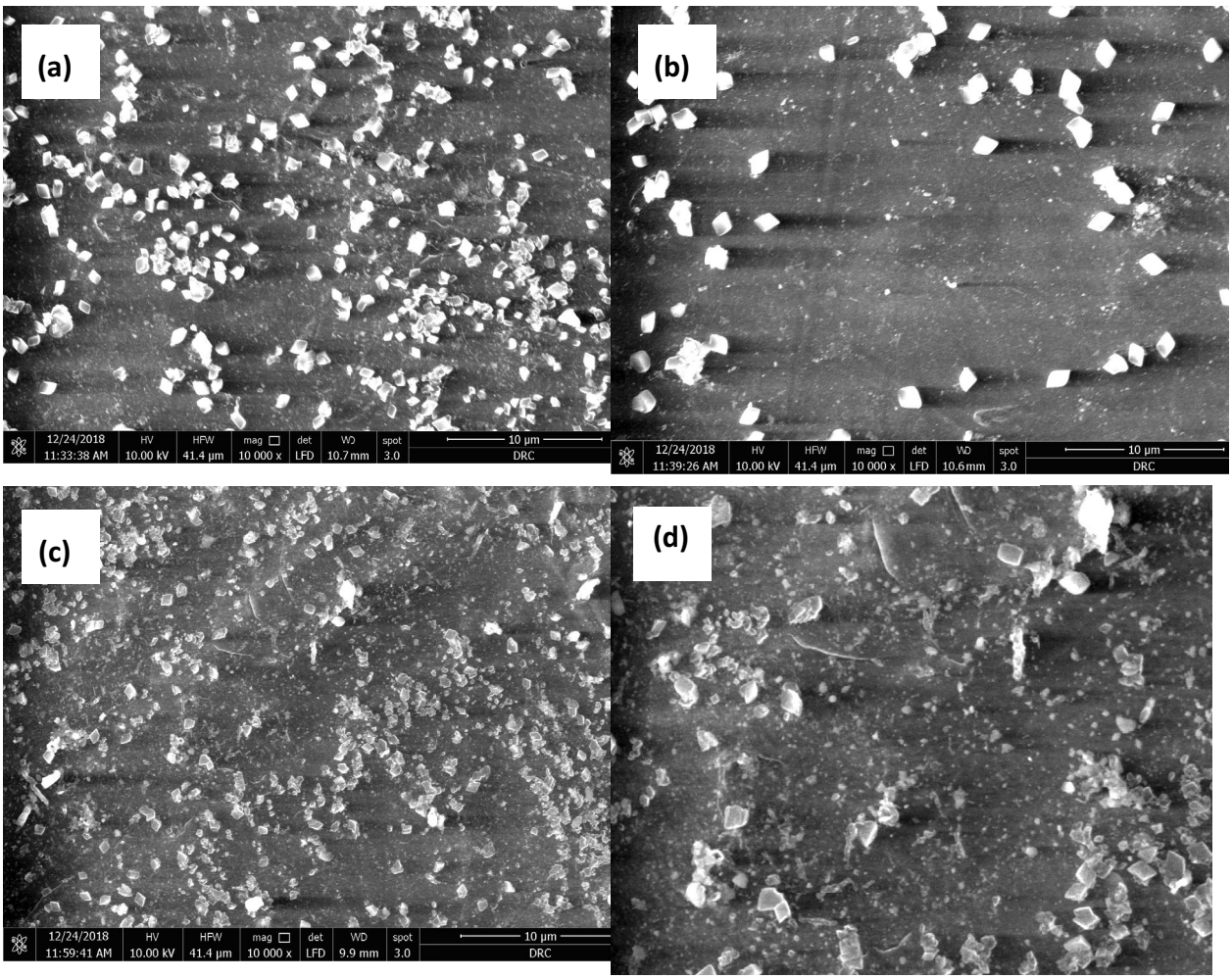

Fig. 12. SEM images showing the adhesion of *E. coli* (a and b) and lesteria (a and d) bacteria on the PSf/PA and Ag/PSf/PA membranes.

onto the PSf support of TFC membranes change their surface roughness and imparted excellent anti-adhesion possessions alongside *E. coli* and *Listeria* sp. indicating the success of silver nanoparticles as an antifouling negotiator.

Acknowledgment

It is a pleasure to acknowledge (Egyptian Desalination Research Center of Excellence (EDRC)), Egypt, Water Desalination Allince project funded by Egyption Academy of Scientific research and Technology.

References

[1] R. Zhang, Y. Liu, M. He, Y. Su, X. Zhao, M. Elimelech, Z. Jiang, Antifouling membranes for sustainable water purification: strategies and mechanisms, Chem. Soc. Rev., 45 (2016) 5888–5924.

[2] B.H. Jeong, E.M. Hoek, Y. Yan, A. Subramani, X. Huang, G. Hurwitz, A.K. Ghosh, A. Jawor, Interfacial polymerization of thin film nanocomposites: a new concept for reverse osmosis membranes, J. Membr. Sci., 294 (2007) 1–7.

[3] W. Lau, S. Gray, T. Matsuura, D. Emadzadeh, J.P. Chen, A. Ismail, A review on polyamide thin film nanocomposite (TFN) membranes: history, applications, challenges and approaches, Water Res., 80 (2015) 306–324.

[4] H. Karkhanechi, F. Razi, I. Sawada, R. Takagi, Y. Ohmukai, H. Matsuyam, Improvement of antibiofouling performance of a reverse osmosis membrane through biocide release and adhesion resistance, Sep. Purif. Technol., 105 (2013) 106–113.

[5] A. Asatekin, A.M. Mayes, Oil industry wastewater treatment with fouling resistant membranes containing amphiphilic comb copolymers, Environ. Sci. Technol., 43 (2009) 4487–4492.

[6] H. Basri, A.F. Ismail, M. Aziz, Polyethersulfone (PES)–silver composite UF membrane: effect of silver loading and PVP molecular weight on membrane morphology and antibacterial activity, Desalination, 273 (2011) 72–80.

[7] D.Y. Koseoglu-Imer, B. Kose, M. Altinbas, I. Koyuncu, The production of polysulfone (PS) membrane with silver nanoparticles (AgNP): physical properties, filtration performances, and biofouling resistances of membranes, J. Membr. Sci., 428 (2013) 620–628.

[8] J. Huang, G. Arthanareeswaran, K. Zhang, Effect of silver loaded sodium zirconium phosphate (nanoAgZ) nanoparticles incorporation on PES membrane performance, Desalination, 285 (2012) 100–107.

[9] A. Mollahosseini, A. Rahimpour, M. Jahamshahi, M. Peyravi, M. Khavarpour, The effect of silver nanoparticle size on performance and antibacteriality of polysulfone ultrafiltration membrane, Desalination, 306 (2012) 41–50.

[10] Y. Liu, X. Wang, F. Yang, X. Yang, Excellent antimicrobial properties of mesoporous anatase TiO_2 and Ag/TiO_2 composite films, Microporous Mesoporous Mater., 114 (2008) 431–439.

[11] H.J. Klasen, A historical review of the use of silver in the treatment of burns. II. Renewed interest for silver, Burns, 26 (2000) 131–138.
[12] I.M. Ali, M.Y. Nassar, Y.H. Kotp, M. Khalil, Cylindrical-design, dehydration, and sorption properties of easily synthesized magnesium phosphosilicate nanopowder, Part. Sci. Technol., 37 (2019) 207–219.
[13] J.H. Li, X.S. Shao, Q. Zhou, M.Z. Li, Q.Q. Zhang, The double effects of silver nanoparticles on the PVDF membrane: surface hydrophilicity and antifouling performance, Appl. Surf. Sci., 265 (2013) 663–670.
[14] Q.H. Tran, A.T. Le, Silver nanoparticles: synthesis, properties, toxicology, applications and perspectives, Adv. Nat. Sci. Nanosci. Nanotechnol., 4 (2013) 4 033001.
[15] A. Ahmad, P. Mukherjee, S. Senapati, D. Mandal, M.I. Khan, R. Kumar, M. Sastry, Extracellular biosynthesis of silver nanoparticles using the fungus *Fusarium oxysporum*, Colloids Surf., B, 28 (2003) 313–318.
[16] N. Vigneshwaran, N.M. Ashtaputre, P.V. Varadarajan, R.P. Nachane, K.M. Paralikar, R.H. Balasubramanya, Biological synthesis of silver nanoparticles using the fungus *Aspergillus flavus*. Mater. Lett., 61 (2007) 1413–1418.
[17] A. Ingle, A. Gade, S. Pierrat, C. Sonnichsen, M. Rai, Mycosynthesis of silver nanoparticles using the fungus *Fusarium acuminatum* and its activity against some human pathogenic bacteria, Curr. Nanosci., 4 (2008) 141–144.
[18] A.A. Ahmed, H. Hamzah, M. Maaroof, Analyzing formation of silver nanoparticles from the filamentous fungus *Fusarium oxysporum* and their antimicrobial activity, Turk. J. Biol., 42 (2008) 54–62.
[19] A. Mukherjee, M. Roy, B.P. Mandal, G.K. Dey, P.K. Mukherjee, J. Ghatak, S.P. Kale, Green synthesis of highly stabilized nanocrystalline silver particles by a non-pathogenic and agriculturally important fungus *T. asperellum*, Nanotechnology, 19 (2008) 075103.
[20] K.S. Hemath Naveen, G. Kumar, L. Karthik, K.V. Bhaskara Rao, Extracellular biosynthesis of silver nanoparticles using the filamentous fungus *Penicillium* sp., Arch. Appl. Sci. Res., 2 (2010) 161–167.
[21] S. Majeed, M.S. Bin Abdullah, G.K. Dash, M.T. Ansari, A. Nanda, Biochemical synthesis of silver nanoprticles using filamentous fungi *Penicillium decumbens* (MTCC-2494) and its efficacy against A-549 lung cancer cell line, Chin. J. Nat. Med., 14 (2016) 615–620.
[22] M. Bawaskar, S. Gaikwad, A. Ingle, D. Rathod, A. Gade, N. Duran, M. Rai, A new report on mycosynthesis of silver nanoparticles by *Fusarium culmorum*, Curr. Nanosci., 6 (2010) 376–380.
[23] V.C. Verma, R.N. Kharwar, A.C. Gange, Biosynthesis of antimicrobial silver nanoparticles by the endophytic fungus *Aspergillus clavatus*, Nanomedicine, 5 (2010) 33–40.
[24] J. Musarrat, S. Dwivedi, B.R. Singh, A.A. Al-Khedhairy, A. Azam, A. Naqvi, Production of antimicrobial silver nanoparticles in water extracts of the fungus *Amylomyces rouxii* strain KSU-09, Bioresour. Technol., 101 (2010) 8772–8776.
[25] E. Castro-Longoria, A.R. Vilchis-Nestor, M. Avalos-Borja, Biosynthesis of silver, gold and bimetallic nanoparticles using the filamentous fungus *Neurospora crassa*, Colloids Surf., B, 83 (2011) 42–48.
[26] K. Vahabi, G.A. Mansoori, S. Karimi, Biosynthesis of silver nanoparticles by fungus *Trichoderma reesei* (a route for large-scale production of AgNPs), Insciences J., 1 (2011) 65–79.
[27] P.C. Nagajyothi, T.V.M. Sreekanth, J.I. Lee, K.D. Lee, Mycosynthesis: antibacterial, antioxidant and antiproliferative activities of silver nanoparticles synthesized from *Inonotus obliquus* (Chaga mushroom) extract, J. Photochem. Photobiol., B, 130 (2014) 299–304.
[28] V. Ahluwalia, J. Kumar, R. Sisodia, N.A. Shakil, S. Walia, Green synthesis of silver nanoparticles by *Trichoderma harzianum* and their bio-efficacy evaluation against *Staphylococcus aureus* and *Klebsiella pneumonia*, Ind. Crops Prod., 55 (2014) 202–206.
[29] P. Phanjom, G. Ahmed, Biosynthesis of silver nanoparticles by *Aspergillus oryzae* (MTCC No. 1846) and its characterizations, Nanosci. Nanotechnol., 5 (2015) 14–21.
[30] D. Amerasan, T. Nataraj, K. Murugan, C. Panneerselvam, P. Madhiyazhagan, M. Nicoletti, G. Benelli, Myco-synthesis of silver nanoparticles using *Metarhizium anisopliae* against the rural malaria vector *Anopheles culicifacies* Giles (Diptera: Culicidae), J. Pest Sci., 89 (2016) 249–256.
[31] M.D. Balakumaran, R. Ramachandran, P. Balashanmugam, D.J. Mukeshkumar, P.T. Kalaichelvan, Mycosynthesis of silver and gold nanoparticles: optimization, characterization and antimicrobial activity against human pathogens, Microbiol. Res., 182 (2016) 8–20.
[32] A.F. El-Baz, A.I. El-Batal, F.M. Abomosalam, A.A. Tayel, Y.M. Shetaia, S.T. Yang, Extracellular biosynthesis of anti-Candida silver nanoparticles using *Monascus purpureus,* J. Basic Microbiol., 56 (2016) 531–540.
[33] P. Azmath, S. Baker, D. Rakshith, S. Satish, Mycosynthesis of silver nanoparticles bearing antibacterial activity, Saudi Pharm. J., 24 (2016) 140–146.
[34] S. Ghanbari, H. Vaghari, Z. Sayyar, M. Adibpour, H. Jafarizadeh-Malmiri, Autoclave-assisted green synthesis of silver nanoparticles using *A. fumigatus* mycelia extract and the evaluation of their physico-chemical properties and antibacterial activity, Green Process. Synth., 7 (2018) 217–224.
[35] A.C.M.S. Barbosa, L.P.C. Silva, C.M. Ferraz, F.L. Tobias, J.V. de Araújo, B. Loureiro, F.R. Braga, Nematicidal activity of silver nanoparticles from the fungus *Duddingtonia flagrans,* Int. J. Nanomed., 14 (2019) 2341–2348.
[36] A.R. de Araujo, J. Ramos-Jesus, T.M. de Oliveira, A.M.A. de Carvalho, P.H.M. Nunes, T.C. Daboit, A. Rodrigues, Identification of Eschweilenol C in derivative of *Terminalia fagifolia* Mart. and green synthesis of bioactive and biocompatible silver nanoparticles, Ind. Crops Prod., 137 (2019) 52–65.
[37] Y.H. Kotp, Removal of organic pollutants using polysulfone ultrafiltration membrane containing polystyrene silicomolybdate nanoparticles: case study: Borg El Arab area, J. Water Process Eng., 30 (2019) 100553.
[38] Y.H. Kotp, Y.A. Shebl, M.S. El-Deab, B.E. El-Anadouli, H.A. Shawky, Performance enhancement of PA-TFC RO membrane by using magnesium silicate nanoparticles, J. Inorg. Organomet. Polym. Mater., 27 (2017) 201–214.
[39] L. Cen, K.G. Neoh, E.T. Kang, Antibacterial activity of cloth functionalized with Nalkylated poly(4-vinylpyridine), J. Biomed. Mater. Res. Part A, 71 (2004) 70–80.
[40] J. Yin, Y. Yang, Z. Hu, B. Deng, Attachment of silver nanoparticles (AgNPs) onto thin-film composite (TFC) membranes through covalent bonding to reduce membrane biofouling, J. Membr. Sci., 441 (2013) 73–82.
[41] L. Wang, R. Chen, Z.F. Ren, C.W. Ge, Z.X. Liu, S.J. He, Y.Q. Yu, C.Y. Wu, L.B. Luo, Plasmonic silver nanosphere enhanced ZnSe nanoribbon/Si heterojunction optoelectronic devices, Nanotechnology, 27 (2016) 215202.
[42] H. Henglein, Colloidal silver nanoparticles: photochemical preparation and interaction with O_2, CCl_4, and some metal ions, Chem. Mater., 10 (1998) 444–450.
[43] M. Abdel-Hameed, M.M.A. ElFadl, M.E. Ali, Y.H. Kotp, H.A. Shawky, Effect of manufacture conditions on reverse osmosis desalination performance of polyamide thin film composite membrane and their spiral wound element, Desal. Water Treat., 69 (2017) 65–71.
[44] S. Mandal, S. Phadtare, M. Sastry, Interfacing biology with nanoparticle, Curr. Appl. Phys., 5 (2005) 118–127.
[45] E.M. Vrijenhoek, S. Hong, M. Elimelech, Influence of membrane surface properties on initial rate of colloidal fouling of reverse osmosis and nanofiltration membranes, J. Membr. Sci., 188 (2001) 115–128.
[46] A.M. Adel, A.M. El-Shafei, A. Ibrahim, M. Al-Shemy, Extraction of oxidized nanocellulose from date palm (*Phoenix dactylifera* L.) sheath fibers: influence of CI and CII polymorphs on the properties of chitosan/bionanocomposite films, Ind. Crops Prod., 124 (2018) 155–165.
[47] A.M. Adel, A.A. Ibrahim, A.M. El-Shafei, M.T. Al-Shemy, Inclusion complex of clove oil with chitosan/β-cyclodextrin citrate/oxidized nanocellulose biocomposite for active food packaging, Food Packag. Shelf Life, 20 (2019) 100307.

[48] A.M. El-Shafei, A.M. Adel, A.A. Ibrahim, M.T. Al-Shemy, Dual functional jute fabric biocomposite with chitosan and phosphorylated nano-cellulose (antimicrobial and thermal stability), Int. J. Biol. Macromol., 124 (2019) 733–741.
[49] J. Zuo, Y. Wang, S.P. Sun, T.S. Chung, Molecular design of thin film composite (TFC) hollow fiber membranes for isopropanol dehydration via pervaporation, J. Membr. Sci., 405 (2012) 123–133.
[50] W. Shao, J.M. Wu, H. Liu, G.H. Dong, S.X. Wang, H.H. Min, M. Huang, Graphene oxide reinforced Ni-P coatings for bacterial adhesion inhibition, RSC Adv., 6 (2016) 46270–46277.
[51] M.M. Said, A.H.M. El-Aassar, Y.H. Kotp, H.A. Shawky, M.S.A. Mottaleb, Performance assessment of prepared polyamide thin film composite membrane for desalination of saline groundwater at Mersa Alam-Ras Banas, Red Sea Coast, Egypt, Desal. Water Treat., 51 (2013) 4927–4937.
[52] H.M. Aly, M.E. Moustafa, E.A. Abdelrahman, Influence of aluminum source on the synthesis of nanosized ZSM-5 zeolite, Der Chem. Sin., 4 (2013) 68–72.
[53] E.A. Abdelrahman, R.M. Hegazey, Facile synthesis of HgO nanoparticles using hydrothermal method for efficient photocatalytic degradation of crystal violet dye under UV and sunlight irradiation, J. Inorg. Organomet. Polym. Mater., 29 (2019) 346–358.
[54] E.A. Abdelrahman, R.M. Hegazey, Exploitation of Egyptian insecticide cans in the fabrication of Si/Fe nanostructures and their chitosan polymer composites for the removal of Ni(II), Cu(II), and Zn(II) ions from aqueous solutions, Composites Part B, 166 (2019) 382–400.
[55] S. Sridhar, T.M. Aminabhavi, S.J. Mayor, M. Ramakrishna, Permeation of carbon dioxide and methane gases through novel silver-incorporated thin film composite pebax membranes, Ind. Eng. Chem. Res., 46 (2007) 8144–8151.
[56] M. Safarpour, A. Khataee, V. Vatanpour, Thin film nanocomposite reverse osmosis membrane modified by reduced graphene oxide/TiO_2 with improved desalination performance, J. Membr. Sci., 489 (2015) 43–54.
[57] L.N. Nthunya, L. Gutierrez, N. Khumalo, S. Derese, B.B. Mamba, A.R. Verliefde, S.D. Mhlanga, Superhydrophobic PVDF nanofibre membranes coated with an organic fouling resistant hydrophilic active layer for direct-contact membrane distillation, Colloids Surf., A, 575 (2019) 363–372.
[58] D.S. Dlamini, B.B. Mamba, J. Li, The role of nanoparticles in the performance of nano-enabled composite membranes–a critical scientific perspective, Sci. Total Environ., 656 (2019) 723–731.
[59] B.J. Trushinski, J.M. Dickson, T. Smyth, R.F. Chids, B.E. McCarry, Polysulfonamide thin-film composite reverse osmosis membranes, J. Membr. Sci., 143 (1998) 181–188.
[60] M. Khayet, J.I. Mengual, Effect of salt concentration during the treatment of humic acid solutions by membrane distillation, Desalination, 168 (2004) 373–381.
[61] S.M. Ghiu, R.P. Carnahan, M. Barger, Mass transfer in RO TFC membranes-dependence on the salt physical and thermodynamic parameters, Desalination, 157 (2003) 385–393.
[62] W. Lawler, Z. Bradford-Hartke, M.J. Cran, M. Duke, G. Leslie, B.P. Ladewig, P. Le-Clech, Towards new opportunities for reuse, recycling and disposal of used reverse osmosis membranes, Desalination, 299 (2012) 103–112.
[63] M.K. da Silva, A. Ambrosi, G.M. dos Ramos, I.C. Tessaro, Rejuvenating polyamide reverse osmosis membranes by tannic acid treatment, Sep. Purif. Technol., 100 (2012) 1–8.
[64] S.T. Mitrouli, A.J. Karabelas, N.P. Isaias, A.S. Al Rammah, Application of hydrophilic macromolecules on thin film composite polyamide membranes for performance restoration, Desalination, 278 (2011) 105–116.
[65] E. Mohamedou, M.Y. Tang, A. Lebkiri, E. Rifi, S. de la Puente Gonzalez, D.B. Penate Suarez, O. Mahmoud, M. Fagel, P. Jaouen, M. Pontie, Autopsie d'une membrane d'osmose inverse usagée prélevée dans le Parc National du Banc d'Arguin (PNBA) en Mauritanie: cas d'étude de Teichitt, J. Water Sci., 23 (2010) 147–158.
[66] E.O. Mohamedou, D.B. Penate Suarez, F. Vince, P. Jaouen, M. Pontie, New lives for old reverse osmosis (RO) membranes, Desalination, 253 (2010) 62–70.
[67] K. Treffry-Goatley, C.A. Buckley, G.R. Groves, Reverse osmosis treatment and reuse of textile dyehouse effluents, Desalination, 47 (1983) 313–320.
[68] X. Shi, G. Tal, N.P. Hankins, V. Gitis, Fouling and cleaning of ultrafiltration membranes: a review, J. Water Process Eng., 1 (2014) 121–138.
[69] J. Nikkola, X. Liu, Y. Li, M. Raulio, H.L. Alakomi, J. Wei, C.Y. Tang, Surface modification of thin film composite RO membrane for enhanced anti-biofouling performance, J. Membr. Sci., 444 (2013) 192–200.